Phase-Only Transmit Beampattern Synthesis With Maximum Mainlobe Gain via Manifold ADMM

Yi Shen, Pengfei Leng, Shengyao Chen, *Member, IEEE*, and Hongtao Li

***Abstract*—Phase-only beampattern synthesis is widely used in radar, communication and other fields, which manipulates only the phases of the array antenna weights to achieve the expected beampattern. This letter proposes a manifold alternating direction method of multipliers-based method to yield phase-only beampattern with mainlobe gain maximization and sidelobe level control, in which the subproblem with phase-only constraint is solved by the Riemannian gradient descent algorithm. Numerical results illustrate that the proposed method can obtain desired beampattern with high mainlobe gain and suppressed sidelobe level. Compared with other representative methods, the proposed method has lower computational time when the antenna number increases.**

***Index Terms*—Alternating optimization, beam synthesis, linear antenna array, phase-only constraint, Riemannian optimization.**

I. Introduction

PHASE-ONLY beampattern synthesis manipulates only the phases of array antenna weights to yield the expected beampattern and keep the excitation magnitudes at a constant. The transmit weights with constant amplitude can maximize the transmit energy efficiency, simplify system reconfiguration, and reduce the system cost [1]. Thus, it is extensively harnessed in radar, wireless communication, and other fields.

The phase-only constraint restricts the feasible region of each transmit weight to a complex unit circle, thus turning the corresponding beampattern synthesis into a nonconvex problem. Several researches have been done to solve it. One of the methods is relaxing the phase-only constraint and turning the problem into a convex problem, which can be solved by readily available solvers such as CVX [2], [3], [4], [5]. In [2], [3], and [4], semidefinite relaxation is adopted but the matrix inverse calculation in literation leads to high computational complexity. In [5], the constant modulus constraint is relaxed to less or equal to 1. However, the method cannot ensure the transmit weight vector always satisfies the phase-only constraint. To address this issue, Zhong et al. [6] proposed a method based on the Riemannian manifold optimization, which interprets the constant modulus constraints as the complex circle manifold. However, it has poor performance in sidelobe suppression and is not applicable to generate shaped beam. In contrast, Khalaj-Amirhosseini [7] provided a method using autocorrelation matching, which can generate beampattern with desired shape, but solving the nonlinear equations needs huge complexity. Due to the decomposability and superior convergence of the alternate direction method of multipliers (ADMM) [11], ADMM-based methods are developed in [8], [9], and [10], which split the original problem into several easy-to-solve subproblems and solve them, respectively. However, the way to solve subproblem such as Broyden–Fletcher–Goldfarb–Shanno (BFGS) algorithm in [8] results in high computational cost when the number of antennas increases. Recently, the neural network is introduced to solve the phase-only beampattern synthesis problem [12], [13], which needs sufficient training data to guarantee the performance.

To obtain good shaped beampattern performance with reduced computational cost, this letter proposes a method based on manifold ADMM (MADMM) [14] for phase-only beampattern synthesis. We aim to maximize the mainlobe gain and to control the sidelobe level (SLL) simultaneously. To achieve this goal, we adopt the ADMM scheme to decompose the original problem into several tractable subproblems. Specifically, we deal with the phase-only constrained subproblems through using Riemannian manifold optimization algorithm. Numerical result shows that the proposed method provides almost the best shaped beampattern performance and consumes the lowest computational cost, especially when the number of antennas grows.

II. Problem Formulation

Consider a uniform linear array with N elements. Its steering vector at the transmit direction $\theta \in [-\pi/2, \pi/2]$ is

$$\boldsymbol{a}(\theta) = \left[A_1(\theta), A_2(\theta)e^{-j2\pi d_2 \sin\theta/\lambda}, \ldots, A_N(\theta)e^{-j2\pi d_N \sin\theta/\lambda}\right]^T \tag{1}$$

where d_n denotes the distance between the nth element and the reference element and λ denotes the signal wavelength. $A_n(\theta)$ is the individual pattern for the nth element. Let $\mathbf{w} = [w_1, w_2, \ldots, w_N]^T$ denote the transmit weight vector. The beampattern can be represented as

$$P(\theta) = \left|\boldsymbol{a}^H(\theta)\mathbf{w}\right|^2. \tag{2}$$

To obtain a desired beampattern with maximum transmit power by phase-only transmit weights, we formulate the original optimization problem as follows:

$$\max_{\mathbf{w},\varepsilon} \varepsilon$$

$$\text{s.t.} \quad \varepsilon \le \left|\boldsymbol{a}^H(\theta_m)\mathbf{w}\right|^2 \le \alpha\varepsilon, \quad m = 1, \ldots, M$$

Manuscript received 10 July 2023; revised 28 August 2023; accepted 24 September 2023. Date of publication 2 October 2023; date of current version 5 January 2024. This work was supported in part by the Key Program of National Natural Science Foundation of China under Grant 41930110 and in part by the Natural Science Foundation of Jiangsu Province under Grant BK20221486. *(Corresponding author: Hongtao Li.)*

Yi Shen, Shengyao Chen, and Hongtao Li are with the School of Electronic and Optical Engineering, Nanjing University of Science and Technology, Nanjing 210094, China (e-mail: shenyi0667@njust.edu.cn; chenshengyao@njust.edu.cn; liht@njust.edu.cn).

Pengfei Leng is with the Nanjing Marine Radar Institute, Nanjing 211153, China (e-mail: lpf_elec@163.com).

Digital Object Identifier 10.1109/LAWP.2023.3321021

$$\begin{aligned} &\left|\boldsymbol{a}^H(\vartheta_s)\mathbf{w}\right|^2 \le \beta_s\varepsilon, \quad s=1,\ldots,S \\ &|w_n| = 1, \quad n=1,2,\ldots,N \end{aligned} \tag{3}$$

where $\{\theta_m\}_{m=1}^M$ and $\{\vartheta_s\}_{s=1}^S$ denotes the discretized angular sets of the mainlobe and sidelobe regions, ε denotes the obtained mainlobe gain, α and $\boldsymbol{\beta}=\{\beta_s\}_{s=1}^S$ is used to control the mainlobe ripple and the sidelobe level. It is notable that the problem (3) is much complicated since all the constraints are nonconvex. In the following, we will provide an effective solution algorithm based on the manifold ADMM.

III. Proposed Method

To simplify the problem (3), we introduce two auxiliary variables $\mathbf{h}=\{h_m\}_{m=1}^M$, $\mathbf{g}=\{g_s\}_{s=1}^S$ to decouple the constraints and define $h_m=\boldsymbol{a}^H(\theta_m)\mathbf{w}$, $g_s=\boldsymbol{a}^H(\vartheta_s)\mathbf{w}$. Then, (3) can be equivalently expressed as

$$\begin{aligned} \min_{\mathbf{w},\varepsilon} \quad & -\varepsilon \\ \text{s.t.} \quad & h_m = \boldsymbol{a}^H(\theta_m)\mathbf{w} \\ & g_s = \boldsymbol{a}^H(\vartheta_s)\mathbf{w} \\ & \varepsilon \le |h_m|^2 \le \alpha\varepsilon, \quad m=1,\ldots,M \\ & |g_s|^2 \le \beta_s\varepsilon, \quad s=1,\ldots,S \\ & |w_n| = 1, \quad n=1,\ldots,N. \end{aligned} \tag{4}$$

To solve the problem (4), we adopt the ADMM scheme. The augmented Lagrangian of (4) is formed as

$$\begin{aligned} &L(\mathbf{w},\varepsilon,\mathbf{h},\mathbf{g},\boldsymbol{\delta},\boldsymbol{\lambda}) \\ &= -\varepsilon + \frac{\rho}{2}\sum_{m=1}^{M}\left(\left|h_m - \boldsymbol{a}^H(\theta_m)\mathbf{w} + \delta_m\right|^2 - |\delta_m|^2\right) \\ &\quad + \frac{\rho}{2}\sum_{s=1}^{S}\left(\left|g_s - \boldsymbol{a}^H(\vartheta_s)\mathbf{w} + \lambda_s\right|^2 - |\lambda_s|^2\right) \end{aligned} \tag{5}$$

where $\rho>0$ is the penalty parameter, $\boldsymbol{\delta}=\{\delta_m\}_{m=1}^M$ and $\boldsymbol{\lambda}=\{\lambda_s\}_{s=1}^S$ are both the scaled dual variables. Based on the principle of ADMM, we resolve the problem (4) by solving the following iterative subproblems:

$$\begin{aligned} \mathbf{w}^{t+1} &= \arg\min_{\mathbf{w}} L\left(\mathbf{w},\varepsilon^t,\mathbf{h}^t,\mathbf{g}^t,\boldsymbol{\delta}^t,\boldsymbol{\lambda}^t\right) \\ &\text{s.t.} \quad |w_n| = 1, \quad n=1,2,\ldots,N \end{aligned} \tag{6a}$$

$$\begin{aligned} \left\{\varepsilon^{t+1},\mathbf{h}^{t+1},\mathbf{g}^{t+1}\right\} &= \arg\min_{\varepsilon,\mathbf{h},\mathbf{g}} L\left(\mathbf{w}^{t+1},\varepsilon,\mathbf{h},\mathbf{g},\boldsymbol{\delta}^t,\boldsymbol{\lambda}^t\right) \\ &\text{s.t.}\ \varepsilon \le |h_m|^2 \le \alpha\varepsilon, \quad m=1,2,\ldots,M \\ &\quad |g_s|^2 \le \beta_s\varepsilon, \quad s=1,2,\ldots,S \end{aligned} \tag{6b}$$

$$\delta_m^{t+1} = \delta_m^t + h_m^{t+1} - \boldsymbol{a}^H(\theta_m)\mathbf{w}^{t+1}, \quad m=1,\ldots,M \tag{6c}$$

$$\lambda_s^{t+1} = \lambda_s^t + g_s^{t+1} - \boldsymbol{a}^H(\vartheta_s)\mathbf{w}^{t+1}, \quad s=1,\ldots,S. \tag{6d}$$

A. Solution to (6a)

Define $\mathbf{A}=[\boldsymbol{a}(\vartheta_1),\ldots,\boldsymbol{a}(\vartheta_S),\boldsymbol{a}(\theta_1),\ldots,\boldsymbol{a}(\theta_M)]^H$ and $u_{1,s}=g_s^t+\lambda_s^t$, $u_{2,m}=h_m^t+\delta_m^t$, $\mathbf{u}=[u_{1,1},\ldots,u_{1,S},u_{2,1},\ldots,u_{2,M}]^T$. Subproblem (6a) can be expressed as the following unit-modulus quadratic programming (UQP) problem

$$\min_{\mathbf{w}} \quad \|\mathbf{u}-\mathbf{A}\mathbf{w}\|_2^2 \quad \text{s.t.}\ |w_n|=1, \quad n=1,\ldots,N. \tag{7}$$

To guarantee the optimal $\mathbf{w}$ strictly satisfy unit-modules constraints, we solve the problem (7) by adopting the Riemannian manifold optimization. Consider the phase-only constraint as a manifold

$$\mathcal{M}_{cc} = \left\{\mathbf{w}\in\mathbb{C}^N : \ w^*(n)w(n)=1, \ \forall n\right\}. \tag{8}$$

The problem (7) is rewritten as

$$\min_{\mathbf{w}\in\mathcal{M}_{cc}} f(\mathbf{w}) \tag{9}$$

where $f(\mathbf{w})=\|\mathbf{u}-\mathbf{A}\mathbf{w}\|_2^2$ denotes the objective function. The Euclidean gradient of $f(\mathbf{w})$ is given by

$$\nabla f(\mathbf{w}) = \mathbf{A}^H\mathbf{A}\mathbf{w} - \mathbf{A}^H\mathbf{u}. \tag{10}$$

By projecting $\nabla f(\mathbf{w})$ onto the tangent space of the manifold $\mathcal{M}_{cc}$ at the point $\mathbf{w}$, the Riemannian gradient of the objective function is obtained as

$$\nabla_{\mathrm{R}} f(\mathbf{w}) = \nabla f(\mathbf{w}) - \mathcal{R}\{\nabla f(\mathbf{w}) \odot \mathbf{w}^*\} \odot \mathbf{w} \tag{11}$$

where $\mathcal{R}\{\boldsymbol{.}\}$ denotes the real parts of the vector and $\odot$ denotes the elementwise multiplication. To minimize $f(\mathbf{w})$ by iteration, the search direction is set to the negative Riemannian gradient, denoted by $\phi=-\nabla_{\mathrm{R}} f(\mathbf{w})$. The $\mathbf{w}$ of the jth iteration is expressed as

$$\mathbf{w}^{j+1} = \left(\mathbf{w}^j + \zeta^j\phi^j\right) / \left|\mathbf{w}^j + \zeta^j\phi^j\right|. \tag{12}$$

The step size ζ can be determined according to the Armijo backtracking line search [15].

The solution to (6a) is summarized in Algorithm 1, where J is the maximum iterative number and ι_w is the stop tolerance.

Algorithm 1: Riemannian Gradient Descent to Solve (6a).

Input: $\mathbf{w}^0$, J, ι_w
While $j<J$ and $\|\mathbf{w}^j-\mathbf{w}^{j-1}\|>\iota_w$ **do**
1: Determine step size ζ by Armijo;
2: Calculate $\nabla_{\mathrm{R}} f(\mathbf{w})$ by (11);
3: Calculate $\mathbf{w}^{j+1}$ by (12);
Loop calculation $j=j+1$
Output: $\mathbf{w}^*=\mathbf{w}^{j+1}$

B. Solution to (6b)

Ignoring the constant term in (6b), the problem is equal to

$$\begin{aligned} \min_{\mathbf{h},\mathbf{g},\varepsilon} \quad & -\varepsilon + \frac{\rho}{2}\sum_{s=1}^{S}|g_s-\hat{g}_s|^2 + \frac{\rho}{2}\sum_{m=1}^{M}\left|h_m-\hat{h}_m\right|^2 \\ \text{s.t.} \quad & |g_s|^2 \le \beta_s\varepsilon, \quad s=1,\ldots,S \\ & \varepsilon \le |h_m|^2 \le \alpha\varepsilon, \quad m=1,\ldots,M \end{aligned} \tag{13}$$

where $\hat{h}_m=\mathbf{a}^H(\theta_m)\mathbf{w}^{t+1}-\delta_m^t$, $\hat{g}_s=\mathbf{a}^H(\vartheta_s)\mathbf{w}^{t+1}-\lambda_s^t$. Apparently, there exists coupling between g_s, h_m, and ε. However, once ε is fixed, we can get the optimal g_s, h_m by solving the following problem:

$$\begin{aligned} \min_{\mathbf{h},\mathbf{g},\varepsilon} \quad & \sum_{s=1}^{S}|g_s-\hat{g}_s|^2 + \sum_{m=1}^{M}\left|h_m-\hat{h}_m\right|^2 \\ \text{s.t.} \quad & |g_s|^2 \le \beta_s\varepsilon, \quad s=1,\ldots,S \\ & \varepsilon \le |h_m|^2 \le \alpha\varepsilon, \quad m=1,\ldots,M. \end{aligned} \tag{14}$$

Obviously, the solution to (14) is

$$h_m = \begin{cases} \hat{h}_m, & \text{if}\sqrt{\varepsilon} \le \left|\hat{h}_m\right| \le \sqrt{\alpha\varepsilon} \\ \sqrt{\varepsilon}\hat{h}_m \Big/ \left|\hat{h}_m\right|, & \text{if}\left|\hat{h}_m\right| < \sqrt{\varepsilon} \\ \sqrt{\alpha\varepsilon}\hat{h}_m \Big/ \left|\hat{h}_m\right|, & \text{if}\left|\hat{h}_m\right| > \sqrt{\alpha\varepsilon} \end{cases} \tag{15}$$

$$g_s = \begin{cases} \hat{g}_s, & \text{if } |\hat{g}_s| \le \sqrt{\beta_s \varepsilon} \\ \sqrt{\beta_s \varepsilon}\hat{g}_s/|\hat{g}_s|, & \text{otherwise.} \end{cases} \tag{16}$$

Inserting (15) and (16) into (13) and let $\varsigma = \sqrt{\varepsilon}$, we have an equivalent problem of (13) only related to the variable ς as follows:

$$\min_{\varsigma} \quad f(\varsigma) = -\varsigma^2 + \frac{\rho}{2}\sum_{s=1}^{S}\omega_s\left(\sqrt{\beta_s}\varsigma - |\hat{g}_s|\right)^2 + \frac{\rho}{2}\sum_{m=1}^{M}\omega'_m\left(\varsigma - \left|\hat{h}_m\right|\right)^2 + \frac{\rho}{2}\sum_{m=1}^{M}\omega''_m\left(\sqrt{\alpha}\varsigma - \left|\hat{h}_m\right|\right)^2 \tag{17}$$

where $\omega_s = 0$ if $|\hat{g}_s| \le \sqrt{\beta_s}\cdot\varsigma$, otherwise, $\omega_s = 1$; $\omega'_m = 0$ if $|\hat{h}_m| \ge \varsigma$, otherwise, $\omega'_m = 1$; $\omega''_m = 0$ if $|\hat{h}_m| \le \sqrt{\alpha}\cdot\varsigma$, otherwise, $\omega''_m = 1$. Define $[v_1 \ldots, v_K]$, $[u_1, \ldots, u_L]$, and $[u'_1, \ldots, u'_L]$ as the ascending order sets of $\{|\hat{g}_s|/\sqrt{\beta_s}\}_{s=1}^{S}$, $\{|\hat{h}_m|\}_{m=1}^{M}$ and $\{|\hat{h}_m|/\sqrt{\alpha}\}_{m=1}^{M}$ with duplicates removed and let $v_0 = u_0 = u'_0 = 0$, $v_{K+1} = u_{L+1} = u'_{L+1} = \infty$. By sorting the set $[v_1, \ldots, v_K, u_1, \ldots, u_L, u'_1, \ldots, u'_L]$ in ascending order and discarding the duplicates, we have the set $[r_1, r_2, \ldots, r_P]$. Let $r_0 = 0$ and $r_{P+1} = \infty$, $f(\varsigma)$ can be transformed into a piecewise function

$$f(\varsigma) = \{f_p(\varsigma) | r_{p-1} \le \varsigma \le r_p, p = 1, \ldots, P+1\}. \tag{18}$$

The pth segment of (18) is expressed as

$$f_p(\varsigma) = a_p\varsigma^2 + b_p\varsigma + c_p \tag{19}$$

where

$$a_p = \frac{\rho}{2}\left(\sum_{i=k'}^{K}\beta_i + \sum_{i=1}^{l'}1 + \sum_{i=l''}^{L}\alpha\right) - 1$$

$$b_p = -\rho\left(\sum_{i=k'}^{K}\sqrt{\beta_i}v_i + \sum_{i=1}^{l'}u_i + \sum_{i=l''}^{L}\sqrt{\alpha}u_i\right)$$

$$c_p = \frac{\rho}{2}\left(\sum_{i=k'}^{K}v_i^2 + \sum_{i=1}^{l'}u_i^2 + \sum_{i=l''}^{L}u_i^2\right) \tag{20}$$

in which k', l' and l'' satisfy $[r_{p-1}, r_p] \subseteq [v_{k'-1}, v_{k'}]$, $[r_{p-1}, r_p] \subseteq [u_{l'}, u_{l'+1}]$, and $[r_{p-1}, r_p] \subseteq [u'_{l''-1}, u'_{l''}]$. Obviously, $f_p(\varsigma)$ is a quadratic function. By choosing appropriate ρ to ensure $a_p > 0$ always holds, the minimal value $f_p(\hat{\varsigma}_p)$ is obtained when $\hat{\varsigma}_p = \arg\min_{\varsigma}\{f_p(r_{p-1}), f_p(r_p), f_p(-b_p/2a_p)\}$.

Sorting the minimum values of $P+1$ segments, we can get the optimal ε^{t+1} represented by

$$\varepsilon^{t+1} = \left\{\arg\min_{\hat{\varsigma}_p}\{f_1(\hat{\varsigma}_1), \ldots, f_{P+1}(\hat{\varsigma}_{P+1})\}\right\}^2. \tag{21}$$

Then, the optimal $\mathbf{g}^{t+1} = \{g_s^{t+1}\}_{s=1}^{S}$ and $\mathbf{h}^{t+1} = \{h_m^{t+1}\}_{m=1}^{M}$ is calculated by inserting ε^{t+1} into (15) and (16).

The complete algorithm to solve (3) is summarized in Algorithm 2.

C. Convergence Analysis

The Riemannian gradient descent method exhibits linear convergence in [16]. The ADMM-based method in Algorithm 2 is proved to converge to a stationary point in [17] if $\lim_{t\to\infty}\boldsymbol{\delta}^{t+1} - \boldsymbol{\delta}^t = \mathbf{0}$ and $\lim_{t\to\infty}\boldsymbol{\lambda}^{t+1} - \boldsymbol{\lambda}^t = \mathbf{0}$ hold. Therefore, the proposed method is convergent under the same conditions.

Algorithm 2: Manifold ADMM to Solve (3).

Initialization: $\mathbf{w}^0$, $\mathbf{h}^0$, $\mathbf{g}^0$, $\boldsymbol{\delta}^0$, $\boldsymbol{\lambda}^0$
While $t < T$ **do**
1: Calculate $\mathbf{w}^{t+1}$ by Algorithm 1;
2: Calculate ε^{t+1}, $\mathbf{g}^{t+1}$ and $\mathbf{h}^{t+1}$ by (21), (15) and (16);
3: Update $\boldsymbol{\delta}^{t+1} = \{\delta_m^{t+1}\}_{m=1}^{M}$, $\boldsymbol{\lambda}^{t+1} = \{\lambda_s^{t+1}\}_{s=1}^{S}$ by (6c) and (6d);
Loop calculation $t = t+1$
Output: $\mathbf{w}^* = \mathbf{w}^{t+1}$

D. Complexity Analysis

Solution to (6a) requires $O\{J(S+M)N^2\}$ multiplications. Solution to (6b) and the update of the dual variables requires $O\{(S+M)N\}$ multiplications/divisions separately. The total complexity in each iteration is dominated by Algorithm 1 and thus is about $O\{J(S+M)N^2\}$. The complexity of the methods in [5] and [8] are denoted as $O\{J'(S+M)N^2\}$ and $O\{\max\{S+M, N\}^4 N^{0.5}\log(1/\varepsilon_{\text{solver}})\}$, where J' denotes the max iteration time of BFGS and $\varepsilon_{\text{solver}}$ denotes the solver tolerance of the CVX toolbox [18]. The specific computation time of each method is provided in the following experiment.

IV. Numerical Results

In this section, we evaluate the performance of the proposed method by several numerical experiments. Consider a uniform line array with 64 antenna elements with half-wavelength element spacing. The antenna elements are isotropic and $A_n(\theta) = 1$. We set $\rho = 1$, $T = 500$ and $\iota_w = 10^{-4}$. The value of $\mathbf{h}^0$, $\mathbf{g}^0$, $\boldsymbol{\delta}^0$, $\boldsymbol{\lambda}^0$ is generated randomly. The value of $\mathbf{w}^0$ has a fixed amplitude equal to 1 and 64 random phases in the interval $[0, 2\pi]$.

A. Case I and II: Focused Beam With Sidelobe Level Control

In *case I*, focused beam is synthesized by the proposed method and methods in [4], [8], and [9]. First, 0° is set as the mainlobe direction and $[-90^\circ, -3^\circ]$ and $[3^\circ, 90^\circ]$ are set as the sidelobe region with -20 dB sidelobe level constraints. All synthesized beampatterns are shown in Fig. 1(a), from which we can see that both the proposed method and [8] can obtain focused beam with sidelobe level control while [5] and [6] cannot control the sidelobe level in the entire sidelobe region. The mainlobe gain obtained by the proposed method is 0.1 dB higher than that obtained by [8]. The minimum SLL of the focused beampattern can achieve -20.01 dB. In *case II*, we consider the situation when radar detects a low altitude weak target. To reduce the ground clutter interference, the sidelobe pointing to the ground should be suppressed sufficiently. Let the mainlobe point at 0°. The sidelobe region $[-90^\circ, -3^\circ]$ pointing to the ground is controlled below -35 dB, while the sidelobe region $[3^\circ, 90^\circ]$ pointing to the airspace is controlled below -10 dB. The beampatterns synthesized by the proposed method and methods in [5], [6], and [8] are shown in Fig. 1(b). It is seen from Fig. 1(b) that the proposed method and that in [5] and [8] can provide expected beampattern, while the method in [6] provides considerably lower mainlobe gain, which leads to a remarkable loss of detection range.

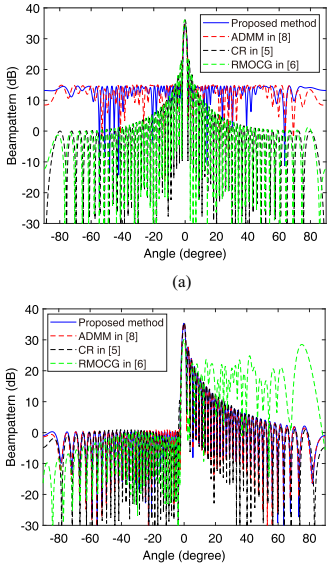

Fig. 1. (a) Focused beampattern in *case I*. (b) Focused beampattern in *case II*.

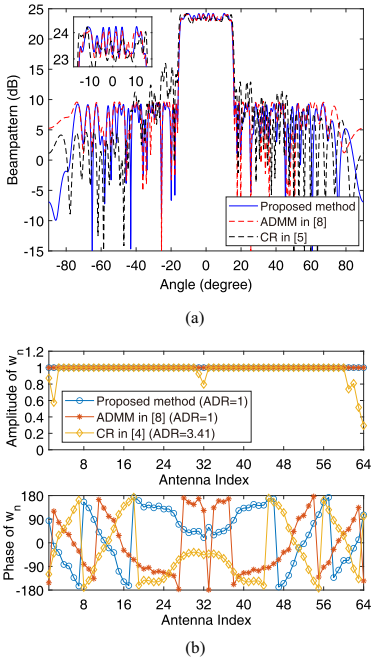

Fig. 2. (a) Shaped beampattern in *case III*. (b) Required amplitude and phase in *case III*.

B. Case III: Shaped Beam With a Wide Mainlobe

Fig. 2(a) displays the shaped beam with a wide mainlobe synthesized by the proposed method and the methods in [5] and [8]. The mainlobe region is set as $[-15^\circ, -15^\circ]$ with a ripple constrain of 1.2 dB. The sidelobe region is set as $[-90^\circ, -16^\circ]$ and $[16^\circ, 90^\circ]$ with a -14 dB sidelobe level constraint. We find that the proposed method can generate the wide mainlobe with lower sidelobe level and flatter mainlobe than that in [5] and provide the mainlobe gain 0.1 dB higher than that in [8]. The minimum SLL of the shaped beampattern can achieve -14.11 dB. Fig. 2(b) shows that the amplitude dynamic range (ADR) generated by the proposed method and that in [8] strictly equals to 1. ADR equals to 3.41 in [5], which means the unit-modules constraint is not satisfied.

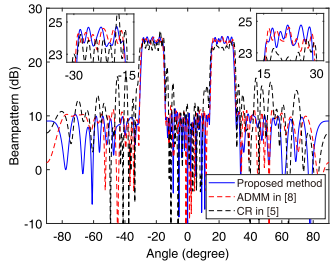

Fig. 3. Shaped beampattern in *case IV*.

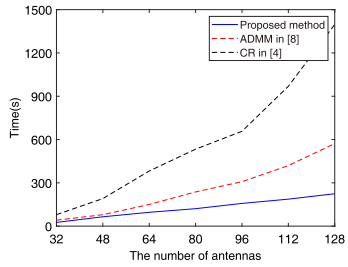

Fig. 4. Computational time analysis.

C. Case IV: Shaped Beam With Multiple Mainlobes

Fig. 3 illustrates the shaped beam with multiple mainlobes synthesized by the proposed method and the methods in [5] and [8]. Two mainlobe regions are set as $[-30^\circ, -15^\circ]$ and $[30^\circ, 15^\circ]$ with 1.4 dB ripple. The sidelobe region are set as $[-90^\circ, -31^\circ]$, $[-14^\circ, 14^\circ]$, and $[31^\circ, 90^\circ]$ with -14 dB sidelobe level. In Fig. 3, we observe that the method in [5] completely lost the ability to control the sidelobe level. In contrast, the proposed method and that in [8] still yield expected multiple mainlobes and sidelobe successfully.

D. Computational Cost

To validate the computational cost of three methods, Fig. 4 shows the CPU time (Intel i9-12900KF CPU, 64 bit, RAM 64 GB) versus the number of antennas for synthesizing shaped beam with the same constraint in *case III*. The proposed method is much faster than that in [5] and [8].

V. Conclusion

In this letter, we proposed a MADMM-based phase-only beampattern synthesis method for maximizing the mainlobe gain and controlling the sidelobe level simultaneously. Based on the principle of MADMM, we translated the original problem into an iterative update containing a UQP problem and a least-squares with variable-coupled box constraints. We then solve the UQP problem by using the Riemannian gradient descent and derive the optimal solution of the proposed least-squares. Numerical results verified that the proposed method yields desired beam-patterns with high mainlobe gain and controlled sidelobe level in several cases and it consumes less computational time than other representative methods.

REFERENCES

[1] A. Y. Gemechu, G. Cui, X. Yu, and L. Kong, "Beampattern synthesis with sidelobe control and applications," *IEEE Trans. Antennas Propag.*, vol. 68, no. 1, pp. 297–310, Jan. 2020.

[2] P. J. Kajenski, "Phase only antenna pattern notching via a semidefinite programming relaxation," *IEEE Trans. Antennas Propag.*, vol. 60, no. 5, pp. 2562–2565, May 2012.

[3] B. Fuchs, "Application of convex relaxation to array synthesis problems," *IEEE Trans. Antennas Propag.*, vol. 62, no. 2, pp. 634–640, Feb. 2014.

[4] Y. Lee, "Adaptive interference suppression of phase-only thinned arrays via convex optimization," *IEEE Trans. Antennas Propag.*, vol. 68, no. 6, pp. 4583–4592, Jun. 2020.

[5] P. Cao, J. S. Thompson, and H. Haas, "Constant modulus shaped beam synthesis via convex relaxation," *IEEE Antennas Wireless Propag. Lett.*, vol. 16, pp. 617–620, 2017.

[6] K. Zhong, J. Hu, Y. Cong, G. Cui, and H. Hu, "RMOCG: A riemannian manifold optimization-based conjugate gradient method for phase-only beamforming synthesis," *IEEE Antennas Wireless Propag. Lett.*, vol. 21, no. 8, pp. 1625–1629, Aug. 2022.

[7] M. Khalaj-Amirhosseini, "Phase-only power pattern synthesis of linear arrays using autocorrelation matching method," *IEEE Antennas Wireless Propag. Lett.*, vol. 18, no. 7, pp. 1487–1491, Jul. 2019.

[8] J. Liang, X. Fan, W. Fan, D. Zhou, and J. Li, "Phase-only pattern synthesis for linear antenna arrays," *IEEE Antennas Wireless Propag. Lett.*, vol. 16, pp. 3232–3235, 2017.

[9] J. Liang, X. Fan, H. C. So, and D. Zhou, "Array beampattern synthesis without specifying lobe level masks," *IEEE Trans. Antennas Propag.*, vol. 68, no. 6, pp. 4526–4539, Jun. 2020.

[10] X. Zhang, J. Liang, X. Fan, G. Yu, and H. C. So, "Reconfigurable array beampattern synthesis via conceptual sensor network modeling and computation," *IEEE Trans. Antennas Propag.*, vol. 68, no. 6, pp. 4512–4525, Jun. 2020.

[11] S. Boyd, N. Parikh, E. Chu, B. Peleato, and J. Eckstein, "Distributed optimization and statistical learning via the alternating direction method of multipliers," *Found. Trends Mach. Learn.*, vol. 3, no. 1, pp. 1–122, 2010.

[12] Z. Zhao, H. Zhao, Z. Wang, M. Zheng, and Q. Xun, "Radial basis function neural network optimal modeling for phase-only array pattern nulling," *IEEE Trans. Antennas Propag.*, vol. 69, no. 11, pp. 7971–7975, Nov. 2021.

[13] S. A. Hamza, M. G. Amin, and B. K. Chalise, "Phase-only reconfigurable sparse array beamforming using deep learning," in *Proc. IEEE Int. Conf. Acoust., Speech Signal Process.*, 2022, pp. 4913–4917.

[14] A. Kovnatsky, K. Glashoff, and M. M. Bronstein, "MADMM: A generic algorithm for non-smooth optimization on manifolds," in *Proc. Eur. Conf. Comput. Vis.*, 2016, pp. 680–696.

[15] L. Armijo, "Minimization of functions having lipschitz continuous first partial derivatives," *Pacific J. Math.*, vol. 16, no. 1, pp. 1–3, 1966.

[16] P.-A. Absil, R. Mahony, and R. Sepulchre, "Line-search algorithms on manifolds," in *Optimization On Matrix Manifolds*. Oxfordshire, U.K.: Princeton Univ. Press, 2007, pp. 63–73.

[17] W. Fan, J. Liang, and J. Li, "Constant modulus MIMO radar waveform design with minimum peak sidelobe transmit beampattern," *IEEE Trans. Signal Process.*, vol. 66, no. 16, pp. 4207–4222, Aug. 2018.

[18] CVX Toolbox: Version 2.2, Jan. 2020. [Online]. Available: http://cvxr.com/cvx/